Applied Microbiology and Biotechnology (2021) 105:3101–3113
https://doi.org/10.1007/s00253-021-11149-6

BIOTECHNOLOGICAL PRODUCTS AND PROCESS ENGINEERING

Enhancing L-malate production of *Aspergillus oryzae* by nitrogen regulation strategy

Lihao Ji[1,2] · Ju Wang[3] · Qiuling Luo[1,2] · Qiang Ding[1,2] · Wenxiu Tang[1,2] · Xiulai Chen[1,2] · Liming Liu[1,2]

Received: 13 November 2020 / Revised: 14 January 2021 / Accepted: 26 January 2021 / Published online: 5 April 2021

Abstract

Regulating morphology engineering and fermentation of *Aspergillus oryzae* makes it possible to increase the titer of L-malate. However, the existing L-malate-producing strain has limited L-malate production capacity and the fermentation process is insufficiently mature, which cannot meet the needs of industrial L-malate production. To further increase the L-malate production capacity of *A. oryzae*, we screened out a mutant strain (FMME-S-38) that produced 79.8 g/L L-malate in 250-mL shake flasks, using a newly developed screening system based on colony morphology on the plate. We further compared the extracellular nitrogen (N1) and intracellular nitrogen (N2) contents of the control and mutant strain (FMME-S-38) to determine the relationship between the curve of nitrogen content (N1 and N2) and the L-malate titer. This correlation was then used to optimize the conditions for developing a novel nitrogen supply strategy (initial tryptone concentration of 6.5 g/L and feeding with 3 g/L tryptone at 24 h). Fermentation in a 7.5-L fermentor under the optimized conditions further increased the titer and productivity of L-malate to 143.3 g/L and 1.19 g/L/h, respectively, corresponding to 164.9 g/L and 1.14 g/L/h in a 30-L fermentor. This nitrogen regulation-based strategy cannot only enhance industrial-scale L-malate production but also has generalizability and the potential to increase the production of similar metabolites.

Key Points

- *Construction of a new screening system based on colony morphology on the plate.*
- *A novel nitrogen regulation strategy used to regulate the production of L-malate.*
- *A nitrogen supply strategy used to maximize the production of L-malate.*

Keywords L-malate · *Aspergillus oryzae* · Screening system · Nitrogen regulation strategy · Nitrogen supply strategy

Introduction

L-malate is a four-carbon carboxylic acid that is widely used in the food, beverage (Kövilein et al. 2019), and pharmaceutical (Ding et al. 2010) industries. L-malate is conventionally produced by chemical synthesis, enzymatic hydration of fumarate, and microbial fermentation from renewable sources. In particular, fermentative L-malate production using bacterial and fungal strains has gained increasing attention owing to its eco-friendly nature and low energy consumption (Chen et al. 2013; Chi et al. 2016; Li et al. 2018b). Several strains can naturally produce L-malate, including some typical model strains, such as *Saccharomyces cerevisiae*, *Escherichia coli*, and *Torulopsis glabrata*, and fungi such as *Schizophyllum commune*, *Aspergillus flavus*, *Zygosaccharomyces rouxii*, *Aspergillus niger*, *Penicillium viticola*, and *Rhizopus delemar* (Table 1).

There has been considerable interest in fermentative L-malate production by engineered *T. glabrata*, *E. coli*, and *S. cerevisiae*. These engineering strategies relate to four pathways. The first pathway is the reductive tricarboxylic acid (rTCA) pathway (with a theoretical yield of 2 mol/mol glucose), in which pyruvate carboxylase and malate dehydrogenase overexpression in *T. glabrata*, *E. coli*, and *S. cerevisiae*

✉ Liming Liu
mingll@jiangnan.edu.cn

[1] State Key Laboratory of Food Science and Technology, Jiangnan University, Wuxi 214122, China

[2] International Joint Laboratory on Food Safety, Jiangnan University, Wuxi 214122, China

[3] College of Food Engineering, Anhui Science and Technology University, Chuzhou 233100, Anhui, China

Table 1 L-malate production by different microorganisms

Strain type	Microrganisms	Titer (g/L)	Productivity (g/L/h)	Fermentation period (h)	Volume of the fermentor	References
Model strains	*Escherichia coli*	51.9	0.72	72	1-L fermentor	Hu et al. (2018)
	Escherichia coli	21.65	0.30	72	5-L fermentor	Dong et al. (2017)
	Escherichia coli	25.8	0.36	72	5-L fermentor	Guo et al. (2018)
	Escherichia coli	34.0	0.47	72	3-L fermentor	Zhang et al. (2011)
	Escherichia coli	36.0	0.60	60	3.6-L fermentor	Gao et al. (2018)
	Escherichia coli	69.1	0.48	144	--	Jantama et al. (2008)
	Saccharomyces cerevisiae	30.3	0.32	94	500-mL shake flask	Chen et al. (2017)
	Saccharomyces cerevisiae	59.0	0.30	192	500-mL shake flask	Zelle et al. (2008)
Filamentous fungi	*Aspergillus flavus*	113	0.59	190	16-L fermentor	Battat et al. (1991)
	Aspergillus niger	201.1	1.05	192	2-L fermentor	Xu et al. (2020)
	Rhizopus delemar	120.5	2.0	60	2-L fermentor	Li et al. (2014)
	Ustilago trichophora	195.0	0.74	263	2.5-L fermentor	Zambanini et al. (2016)
	Penicillium viticola	168.0	1.75	96	10-L fermentor	Khan et al. (2014)
	Aspergillus.oryzae	142.5	1.08	132	30-L fermentor	Chen et al. (2019)
	Aspergillus.oryzae	154.0	0.94	164	2-L fermentor	Brown et al. (2013)
	Aspergillus.oryzae	165.0	1.38	120	3-L fermentor	Liu et al. (2017)
	Aspergillus.oryzae	164.9	1.14	144	30-L fermentor	This study

leads to L-malate yields of 8.5 g/L, 34.0 g/L, and 59.0 g/L, respectively (Chen et al. 2013; Zelle et al. 2008; Zhang et al. 2011). The second pathway is the classic TCA cycle (with a theoretical yield of 1.0 mol/mol glucose), in which oxaloacetate and acetyl-CoA enter the TCA cycle through citric acid synthesis and then synthesize L-malate (Iyyappan et al. 2019). The third pathway is the glyoxylate cycle (with a theoretical yield of 1.33 mol/mol glucose), which has received relatively less attention; this pathway involves multiplex tuning of a five-enzyme cascade reaction in the glyoxylate pathway from pyruvate to malate, thereby increasing the L-malate titer to 36 g/L (Gao et al. 2018) (Table 1). The fourth pathway is the one-step synthesis pathway (with a theoretical yield of 2 mol/mol glucose), in which the malic enzyme is introduced into *E. coli* W3110, and the strain is optimized to increase the L-malate titer to 21.65 g/L (Dong et al. 2017). Among these, due to its higher theoretical L-malate yield of 2 mol/mol, the rTCA pathway is the most promising one for L-malate production.

For the natural producers of L-malate (Adrio & Demain 2006), including the filamentous fungi *A. flavus*, *A. niger*, *R. delemar*, *Aspergillus oryzae*, *Ustilago trichophora*, and *Penicillium viticola* can produce ≥100 g/L L-malate in fermentation broth, and these producers have been investigated for decades (Table 1). Among them, *A. oryzae*, a (GRAS) strain that is "generally regarded as safe," can utilize the rTCA pathway for the industrial synthesis of L-malate (Brown et al. 2013). In order to further increase the titer of L-malate produced by *A. oryzae*, a series of strategies, such as random mutagenesis, fermentation optimization, and metabolic engineering, has been developed. For example, in our previous study, a combined mutagenesis strategy using atmospheric and room temperature plasma (ARTP), ^{60}Co-γ, and diethyl sulfate (DES) irradiation was established to isolate the high-yielding *A. oryzae* strain FMME218-37 (46.72 g/L) (Ding et al. 2018). The optimization of fermentation focuses on two aspects: regulating the agitation speed and aeration rate to manipulate the *A. oryzae* morphology, thus increasing the L-malate titer to 142.5 g/L (Chen et al. 2019), and changing the ratio of carbon-to-nitrogen (C/N) in fermentation broth from 150:1 to 50:1, thereby further increasing the L-malate titer by 63.0% (Ding et al. 2018). For metabolic engineering, pyruvate carboxylase and malate dehydrogenase in the rTCA pathway and the C4-dicarboxylate transporter were overexpressed in two different studies, and the L-malate titer was increased to 154 g/L and 165 g/L, respectively (Brown et al. 2013; Liu et al. 2017). However, engineered filamentous fungi typically exhibit transcription instability (Wakai et al. 2014), low homologous recombination efficiency (<5%) (Kuck & Hoff 2010), relatively poor cell growth, and lower stress tolerance (Karahalil et al. 2019), which limits their application on an industrial scale.

Nitrogen is an essential element for filamentous fungi growth and metabolite synthesis, and the demand for nitrogen varies greatly at different stages of growth and product synthesis (Kuypers et al. 2018). Therefore, most of the research on fermentation engineering has focused on optimizing the

nitrogen type, concentration, and C/N ratio to maximize the titer of targeted products (Christensen et al. 1998; Knuf et al. 2013; Rokem et al. 2007; Zhang et al. 2007). However, these studies have generally ignored the differences in nitrogen requirements at the growth and product synthesis stages. Furthermore, the relationship between the change in nitrogen content and product synthesis during different fermentation stages has not yet been clarified, which has largely hindered any further increase in the yielded L-malate titer. In this study, a novel screening system based on colony morphology was developed, and the high L-malate-producing mutant FMME-S-38 was isolated. Based on this, the relationship between nitrogen utilization and L-malate synthesis by mutant FMME-S-38 was elucidated in a 7.5-L fermentor. A novel nitrogen supply strategy was developed, resulting in an increase in the L-malate titer from 130.1 to 164.9 g/L in a 30-L fermentor.

Materials and methods

Strain and culture conditions. The parent strain *A. oryzae* FMME218-37 and the mutant *A. oryzae* FMME-S-38 were conserved in China Center for Type Culture Collection (CCTCC), with preservation number of CCTCC NO: M 2016401 and NO: M 2020294. Sporulation medium was composed of potato extract 500 g/L, glucose 20 g/L, agar 20 g/L. The screening plate medium was composed of $(NH_4)_2SO_4$ 6 g/L, K_2HPO_4 0.525 g/L, KH_2PO_4 0.525 g/L. Seed medium was composed of 60 g/L glucose, 3 g/L yeast powder, 750 mg/L KH_2PO_4, 980 mg/L $K_2HPO_4{\cdot}3H_2O$, 100 mg/L $MgSO_4{\cdot}7H_2O$, 75 mg/L $CaCl_2$, and 1 mL/L ×1000 micronutrient solution (5 g $ZnSO_4$, 5 g NaCl, 5 g $FeSO_4{\cdot}7H_2O$, 1 L water). Acid production medium in 250-mL shake flask was composed of 80 g/L glucose, 30 g/L $CaCO_3$, 3 g/L tryptone, 600 mg/L KH_2PO_4, 600 mg/L $K_2HPO_4{\cdot}3H_2O$, 100 mg/L $MgSO_4{\cdot}7H_2O$, 75 mg/L $CaCl_2$, 8 mg/L $MnSO_4$, and 1 mL/L ×1000 micronutrient solution, feeding glucose 30 g/L and $CaCO_3$ 30 g/L every 48 h. Acid production medium in 7.5-L fermentor was composed of 130 g/L glucose, 30 g/L $CaCO_3$, 6 g/L tryptone, 600 mg/L KH_2PO_4, 600 mg/L $K_2HPO_4{\cdot}3H_2O$, 100 mg/L $MgSO_4{\cdot}7H_2O$, 75 mg/L $CaCl_2$, 8 mg/L $MnSO_4$, and 1 mL/L ×1000 micronutrient solution.

After 4 days of strain growth on the sporulation and screening plates at 35 °C, the mature colonies were collected using 0.05% Tween solution and obtained spore suspension. The spore suspension was sonicated using an Ultrasonic Cell Disruptor (power 285W, 4 s pulse, 4 s pause, total 10 min). The collected spore suspension was inoculated into seed medium in 1.5×10^8 spores/mL, and the culture temperature and culture time were 34 °C and 24 h, respectively, which were cultured in 500-mL unbaffled flasks containing 150-mL media. Shake flask fermentations were inoculated with 10% seed medium in 250-mL shake flask with 50 mL working volumes and were cultured at 36 °C with shaking at 200 rpm for 120 h, feeding 60 g/L $CaCO_3$ and 60 g/L glucose.

In the research, 7.5-L fermentor (INFORS infors, Switzerland) and 30-L fermentor (INFORS techfors, Switzerland) with 50% working volume were used for fermentation evaluation, and the inoculation concentration was the same as shake flask. A two-stage temperature controlling strategy was used to control the fermentation temperature (36 °C at first 18 h and 32 °C until 120 h). The agitation speed is 600 pm until 144 h. During the first 72 h, 40 g/L $CaCO_3$ was added every 24 h to maintain the pH over 6.0 and the glucose was added in a constant flow to maintain the glucose concentration over 25 g/L. All the *A.oryzae* mutants used the same culture conditions.

ARTP, ^{60}Co-γ, and NTG mutagenesis. Spores were collected from the PDA plate after 3–4 days and then washed with demineralized water. The procedures for ^{60}Co-γ irradiation and atmospheric and room temperature plasma (ARTP) were performed as described previously (Ding et al. 2018). For NTG mutagenesis, the suspended spores were treated with 1 mg/mL to cause mutagenesis, and cultured in an oscillator at 34 °C for 1 min (Harper & Lee 2012; Huang et al. 2019; Lim et al. 2019).

Morphology characterization. Morphology characteristics of colonies were determined by the camera (Nikon D70, Nikon Corporation, Japan). The spores and mycelium were determined by scanning electron microscope (SEM, FEI Company, Quanta-200), which were cultured for 84 h at 35 °C on potato dextrose agar (PDA). The pellets in the 7.5-L and 30-L fermentor were determined by iBright™ imaging system (Thermo Fisher Scientific Company, America). The pellets and pellets mycelium were cultured for 120 h in a 7.5-L fermentor or 30-L fermentor at 32 °C.

Enzyme analysis. The sample preparation was determined as described previously (Knuf et al. 2013). Malate dehydrogenase and pyruvate carboxylase activity were determined as proposed in a previous study (Knuf et al. 2013). Glutamate synthase (GOGAT), glutamine synthase (GS), and glutamate dehydrogenase (GDH) were determined in a previous study (Downes et al. 2013).

Nitrogen content detection. The centrifuged samples (12,000 g, 10 min) of fermentation broth were filtered through 0.22-μm filters. For analysis of extracellular nitrogen content, 10 mL sulfuric acid was used to convert organic nitrogen into ammonia and combined to form ammonium sulfate. Besides, 40% NaOH was added to made ammonia distill out which absorbed with boric acid and then titrated with 0.01% standard hydrochloric acid

solution. Using Kjeldahl nitrogen meter to determine the extracellular nitrogen content (Battat et al. 1991).

The pellets in the broth were collected and washed 3–4 times using sterile water. Furthermore, the washed pellets were treated with 2M HCl to dissolve the calcium carbonate on the surface, and further use the freeze-drying technique to remove the water in pellets. Finally, the samples were ground to a smooth powder using a sterilized mortar. Using the same method as the extracellular nitrogen content to determine the intracellular nitrogen content.

Analytical methods. The determination of glucose concentration, dry cell weight, and L-malate concentration were reported in our previous research (Ding et al. 2018).

Results

Isolation of high L-malate-producing mutants based on morphological characterization

In a previous study, it was found that the L-malate titer shows a close correlation with *A. oryzae* colony morphology (Chen et al. 2019; Ding et al. 2018). A high-producing strain should exhibit four features: (i) a larger colony diameter (Fig. 1a); (ii) a lower percentage of vegetative mycelia (white, non-conidiating mycelia), which was previously defined as PVM (Kowalski et al. 2019) (Fig. 1b); (iii) a larger color-changing circle (Fig. 1c); and (iv) denser spore concentration in the colony (Fig. 1d). In order to isolate the high L-malate-producing *A. oryzae* strain, three-round combined mutagenesis consisting of ARTP, ^{60}Co-γ, and NTG was used. Firstly, a mutant library, containing over 400 mutants, was constructed by ARTP, and 50 target mutants were identified that met the four features of high L-malate-producing strains on the screening plate. Among them, amount of the mutant FMME 446 that could produce 59.5 g/L L-malate was found to be 43.0% higher than that of the parent strain (Fig. 2a). In the second round of screening, ^{60}Co-γ irradiation was applied to the mutant FMME 446 and a new mutant library (>400 mutants) was built, which was narrowed down to 50 candidates according to colony morphology. Ultimately, the FMME 432 mutant was screened, and the L-malate titer increased to 74.3 g/L; this amount was 23.4% higher than that of FMME 446 (Fig. 2a).

However, with progressing mutagenesis, the morphological convergence of the mutants gradually increased, which ultimately decreased the efficiency of colony-based screening method (Fig. 2b3, b4). Therefore, 0.02 g/L cycloheximide was added to the plate to discriminate the morphological differences among mutant strains (Adrio & Demain 2006; Swift et al. 2000). As a result, the FMME-S-38 mutant was isolated according to its advantageous morphological traits. FMME-S-38 produced 79.8 g/L L-malate, which was 7.4%, 34.1%, and 91.8% higher than that produced by FMME 432, FMME 446, and the parent strain, respectively. It was found that (1) the colony diameter of *A. oryzae* FMME-S-38 reached 42 mm, which was 1.4-fold higher than that of the parent strain (Fig. 2b1, b4); (2) compactness of the colony was high, and its PVM was the lowest (only 28.9%) (Fig. 2b5, b8); and (3) diameter of the color-changing circle reached 69 mm, which was 2.1-fold higher than that of the parent strain (Fig. 2b9, b12). Finally, scanning electron microscopy showed that the conidial head of mutant FMME-S-38 was plumper and concentrated (Fig. 2b13, b16) and its conidiophore was rougher and had more spikes than that of the parent strain (Fig. 2b17, b20).

In a 7.5-L fermentor, the titer, yield, and productivity of L-malate by the mutant FMME-S-38 were 110.2 g/L, 0.73 g/g, and 0.92 $g \cdot L^{-1} \cdot h^{-1}$, respectively, and these were 54.7%, 37.7%, and 55.9% higher than the corresponding values of the parent strain. The dry cell weight (DCW) and pellet number of mutant FMME-S-38 increased by 50% and 74.13%, respectively, whereas the pellet size decreased by 26.23% compared with those of the parent strain. Moreover, the nitrogen consumption of mutant FMME-S-38 was 1.24-fold higher than that of the parent strain, which may explain its increased L-malate accumulation (Table 2; Fig. 2c).

Elucidation of the correlation between nitrogen utilization and L-malate production

The effect of nitrogen utilization on the accumulation of L-malate is summarized in Fig. 3a, b. The extracellular nitrogen (N1) and intracellular nitrogen (N2) contents of mutant FMME-S-38 were detected in 7.5-L fermentors at 6-h intervals (Fig. 3a, b). The N1 level first decreased rapidly at 0–24 h of fermentation, steadily decreased to reach the lowest point 90 h later, and then substantially increased to 0.0321% thereafter (Fig. 3a). By contrast, the N2 level first increased sharply to 0.231% at 0–24 h and then steadily increased to its peak value (0.375%) at 90 h, followed by a decrease to 0.312%. Considering the change in L-malate productivity at different fermentation stages, the process of L-malate fermentation was divided into three stages: (i) the fungal growth period, in which N1 rapidly declines while N2 increases for biomass formation (Fig. 3a, b), thus leading to slight L-malate accumulation; (ii) the rapid acid-producing period, in which the L-malate titer sharply increases, with N1 and N2 changing only slightly (Fig. 3a); and (iii) the self-dissolving stage, during which N1 steadily increases due to protease secretion and autolysis, while N2 and L-malate production decreases (Fig. 3a). Similar trends were also detected in the case of the parent strain (Fig. 3b). Although the growth stage of both strains lasted about 24 h, the time at which the lowest level of N1 (T_{N1}) and the highest level of N2 (T_{N2}) were detected, varied greatly between the strains (Fig. 3c, d). These two factors are

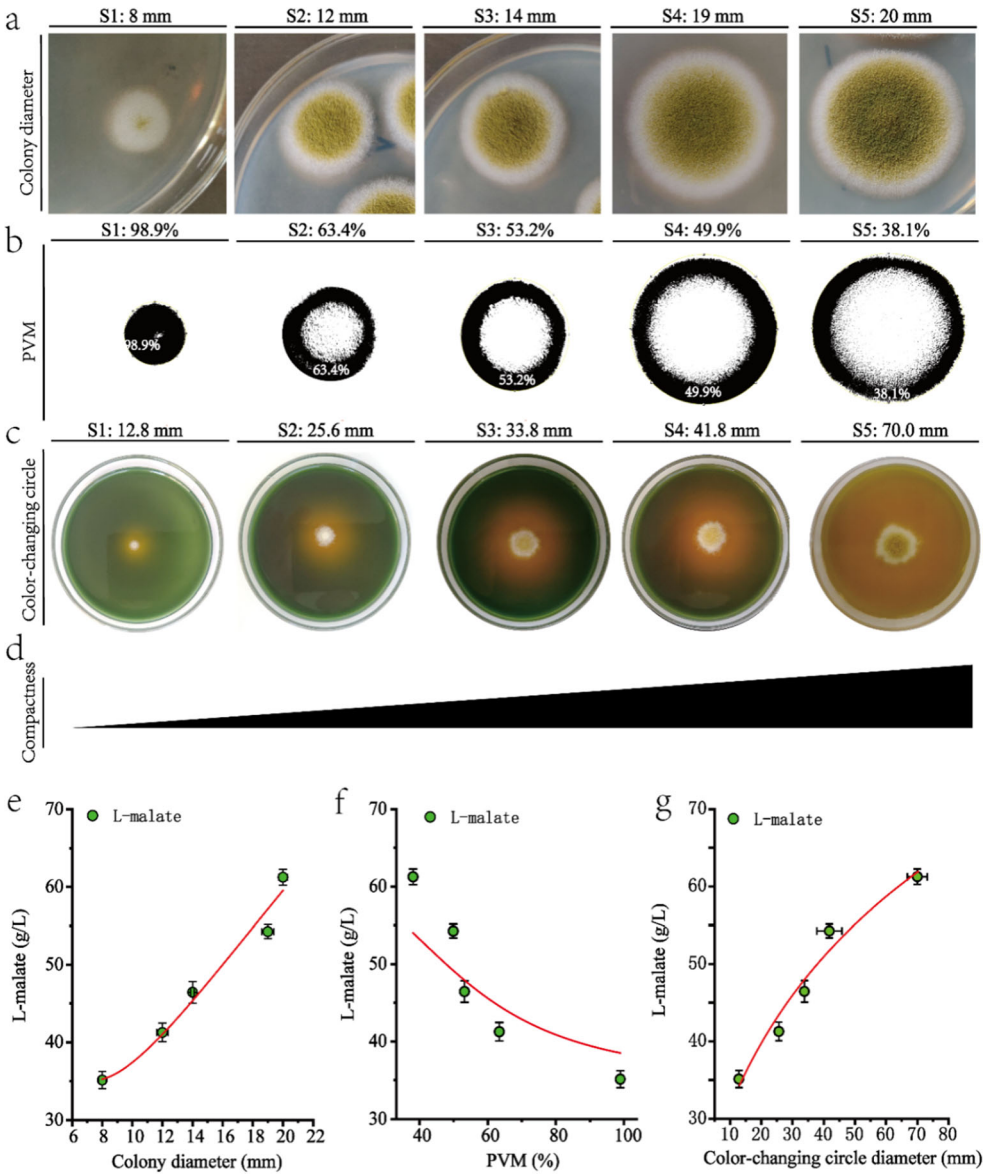

Fig. 1 Correlation between colony morphology and L-malate titer in *Aspergillus oryzae*. **a** Colony diameter of five selected mutants. **b** Percentage of vegetative mycelia (PVM) of the five selected mutants. **c** Color-changing circle diameter of the five selected mutants. **d** Compactness of the five selected mutants. **e** Relationship between the colony diameter and L-malate titer. **f** Relationship between PVM and L-malate titer. **g** Relationship between color-changing circle diameter and L-malate titer

important indicators of the rapid acid-producing period. In mutant FMME-S-38, the T_{N1} and T_{N2} values were reached at 90 h, which is longer than the time required in the parent strain, i.e., 36 h and 48 h, respectively (Fig. 3e, f). This extended period results in a longer acid production period and a shorter self-dissolving period, which ultimately increases the L-malate titer. Therefore, it was hypothesized that the increase in T_{N1} and T_{N2} values could increase the L-malate titer of the mutant FMME-S-38.

To further verify this hypothesis, the specific activities of key enzymes in nitrogen and carbon metabolism were determined, as illustrated in Fig. 3e, h. In the carbon metabolism pathway, the activities of malate dehydrogenase (MDH) and pyruvate carboxylase (PYC) in mutant FMME-S-38 were both higher than those in the parent strain, which accounted for the higher L-malate production by the mutant FMME-S-38 (Fig. 3g, h). Moreover, MDH activity peaked at 48 h, which was a key turning point for the sharp increase in L-malate productivity (Fig. 3g). In the nitrogen metabolism pathway, mutant FMME-S-38 consistently exhibited higher glutamine synthase (GS) and glutamate synthase (GOGAT) activities than the parent strain, indicating a higher N1 consumption rate and DCW (Fig. 3i, j). The nitrogen content in the fungal growth period was mainly allocated to biomass formation, which is a process that depends on the rapid use of N1 to accumulate N2, explaining the sharp decrease in N1 value (Fig. 3a). Consequently, the GS and GOGAT activities in the first 48 h increased rapidly and peaked at 48 h (Fig. 3i, j). When the strain entered the rapid acid production period, the dependence on N1 consumption was reduced, leading to notable decrease in the activities of GS and GOGAT after 48 h (Fig. 3i, j); meanwhile, the N1 and N2 levels remained

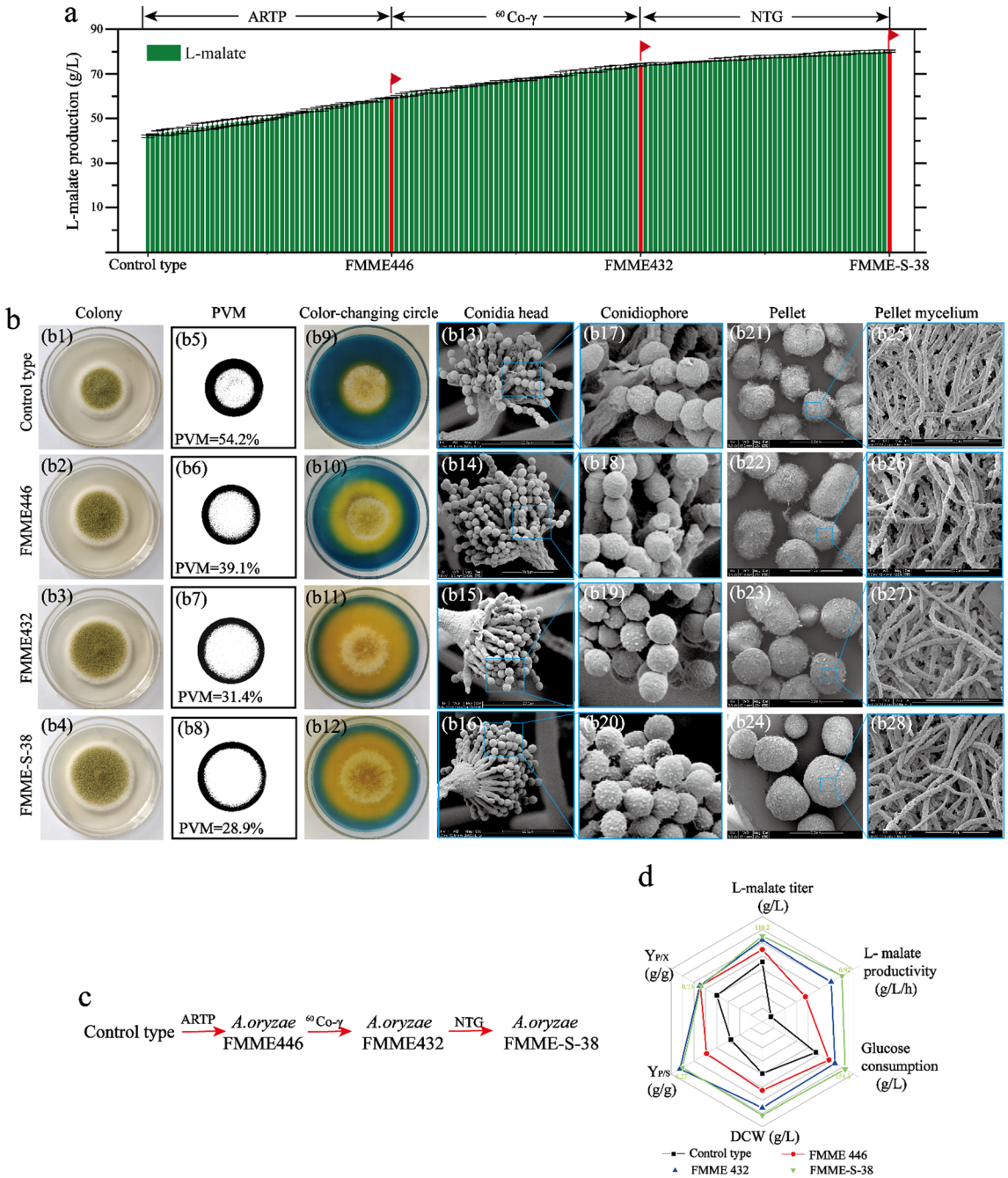

Fig. 2 The screening system was constructed based on a morphological engineering strategy. **a** The mutant library was constructed by ARTP irradiation, ^{60}Co-γ irradiation, and NTG-mediated mutagenesis. The bar chart in red shows the high-producing strains screened by each round of mutagenesis. **b** Images of the colonies (b1–b4), percentage of vegetative mycelia (PVM) of colonies (b5–b8), conidia head (b9–b12), conidiophore (b13–b16), pellet (b17–b20), and pellet mycelium (b21–b24) of the four mutants. **c** Flow chart of three-round compound mutagenesis. **d** The fermentation parameters of the control (FMME218-37), FMME446, FMME432, and FMME-S-38 strains in a 7.5-L fermentor

steady. Furthermore, there was a slight increase in GOGAT activity at 96 h (Fig. 3j), which may be explained by appearance of the self-dissolving stage, with N1 rising and N2 decreasing slightly (Fig. 3a, b). Therefore, the correlation between T_{N1}, T_{N2}, and L-malate production could be easily monitored during the process of fermentation.

Enhancing L-malate production by elevating the T_{N1} value

Based on these results, an external nitrogen supply strategy, involving the initial tryptone content, the feeding tryptone concentrations, and the feeding time of tryptone, was

Table 2 Comparison of fermentation profile of the parent strain and *A.oryzae* FMME-S-38 in the shake flask

Parameter	Strains				Change rate (%)		
	Parent strain (A)	FMME 446 (B)	FMME 432 (C)	FMME-S-38 (D)	(B-A)/A ×100%	(C-A)/A ×100%	(D-A)/A ×100%
Culture time (h)	120	120	120	120	-		
Glucose consumption (g/L)	133.2±1.2	141.3±0.8	145±1.3	151.3±0.6	6.08	8.86	13.59
DCW (g/L)	11.98±0.6	14.26±0.8	16.59±0.4	17.58±0.8	19.03	38.48	46.74
Pellet size diameter (mm)	1.22±0.25	1.14±0.14	1.01±0.10	0.9±0.02	−6.56	−17.21	−26.23
Pellet number (/mL)	201±6	246±8	316±4	350±6	22.39	57.21	74.13
L-malate titer (g/L)	71.2±1.0	89.6±0.9	104.3±0.5	110.2±0.5	25.84	46.49	54.78
L-malate productivity)g/(L·h))	0.59	0.75	0.87	0.92	27.12	47.46	55.93
$Y_{P/S}$[a](g/g)	0.53	0.63	0.74	0.73	18.87	39.62	37.74
$Y_{P/X}$[b](g/g)	5.94	6.28	6.29	6.27	5.72	5.89	5.56
$Y_{X/S}$[c](g/g)	0.09	0.101	0.114	0.116	12.22	26.67	28.89
Nitrogen consumption (%)	0.0472	0.0483	0.0530	0.0583	2.33	12.29	23.52

The numbers stated are means of three individual experiments± standard errors

[a] $Y_{P/S}$ yield of L-malate per substrate

[b] $Y_{P/X}$ yield of L-malate per DCW

[c] $Y_{X/S}$ yield of DCW per DCW

suggested to increase the T_{N1} value. When the initial tryptone content was increased from 5.5 to 7.5 g/L, the T_{N1} value firstly increased from 48 h (5.5 g/L tryptone) to 90 h (6.5 g/L tryptone) (Fig. 4a, b). As a result, the L-malate titer, pellet number, DCW, and consumed glucose increased by 36.4%, 30.9%, 59.2%, and 44.9%, respectively (Fig. 4g-i). Effect of the feeding tryptone concentrations (1 to 5 g/L) on the T_{N1} value and the L-malate titer is demonstrated in Fig. 4c, d. It was found that the T_{N1} value first increased from 66 h to 96 h, and then decreased to 42 h, with an increase in the tryptone feeding concentration from 1 to 5 g/L. The highest L-malate titer (140.6 g/L) was achieved at the maximal T_{N1} value of 96 h, when 3 g/L tryptone was fed into the fermentation broth. When the feeding time of 3 g/L tryptone was delayed from 12 to 36 h, the T_{N1} value first increased from 42 h to 102 h and then decreased to 66 h. As a result, the L-malate titer first increased from 99.6 to 143.3 g/L and then decreased to 116.9 g/L (Fig. 4e, f). The highest titer of L-malate was 143.3 g/L in the 7.5-L fermentor when feeding 3 g/L tryptone at 24 h, and the T_{N1} value reached 102 h (Fig. 4m, o). Therefore, it can be concluded that the L-malate titer could be further increased by changing the T_{N1} value. Moreover, the optimum conditions for the nitrogen supply strategy were the initial tryptone concentration of 6.5 g/L and feeding 3 g/L tryptone at 24 h.

Scaling up in a 30-L fermentor

Using the optimum nitrogen supply strategy in a 30-L fermentor, the T_{N1} value of the mutant FMME-S-38 increased from 78 to 114 h, which was higher than that obtained in the 7.5-L fermentor. Furthermore, there was a corresponding increase in the T_{N2} value from 84 to 108 h (Fig. 5a, b). The L-malate titer, yield, and productivity reached 164.9 g/L, 0.77 g/g, and 1.14 $g{\cdot}L^{-1}{\cdot}h^{-1}$, which were 26.7%, 24.2%, and 27.8% higher, respectively, than the corresponding values when the optimal nitrogen supply strategy was not used (Fig. 5c, d). Furthermore, the DCW increased from 26.19 to 30.10 g/L, while glucose consumption increased from 182 to 207 g/L (Fig. 5c, d). The number of pellets increased from 335 to 380/mL, with the diameter decreasing from 0.86 to 0.74 mm (Fig. 5e). These results indicate that the optimum nitrogen supply strategy is promising for enhancing L-malate production by *A. oryzae*.

Discussion

To further increase the titer, yield, and productivity of L-malate by *A. oryzae* for industrial-scale production, a high L-malate -producing mutant strain (FMME-S-38) was isolated by determining the correlation between colony morphology and the L-malate titer. The fermentation process of the mutant FMME-S-38 was separated into three stages to establish the correlations between the N1 and N2 content and the L-malate titer. Based on this correlation, a novel nitrogen supply strategy was developed to further increase the L-malate titer in both 7.5-L and 30-L fermentors. Our results provide a new

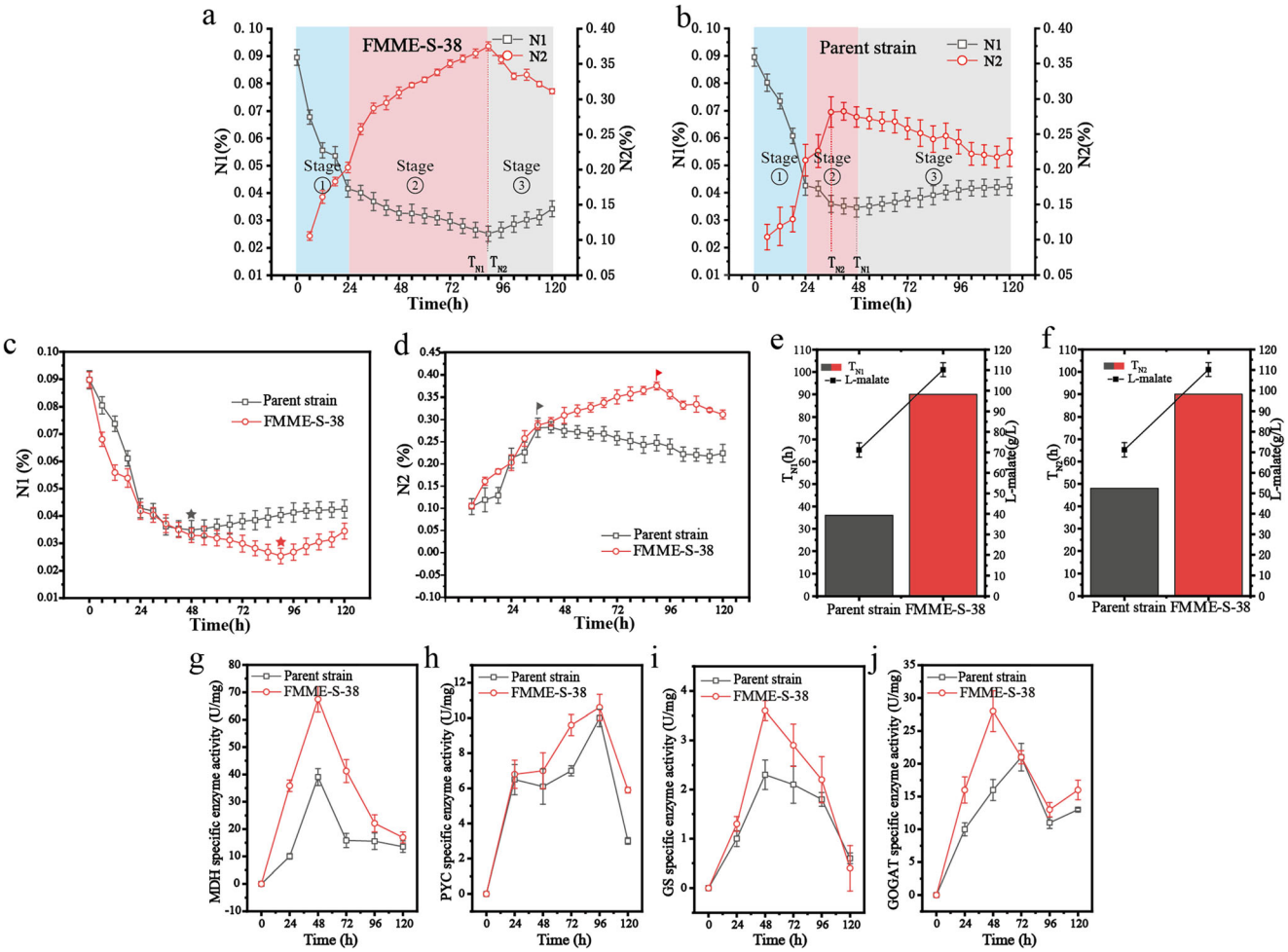

Fig. 3 Correlation between nitrogen utilization and L-malate production. **a**–**b** Different stages of the fermentation process of the mutant strain FMME-S-38 and the parent strain: stage 1, growth stage (highlighted in blue); stage 2, rapid acid-producing period (highlighted in pink); stage 3, self-dissolving stage (highlighted in grey). **c**–**d** The curves of extracellular nitrogen content (N1) and intracellular nitrogen content (N2) of the four strains for 120 h. The lowest point of N1 is represented as a solid five-pointed star, and the highest point reached for N2 is represented as a solid flag symbol. **e-f** The relationship between T_{N1}, T_{N2} values and L-malate production is presented as a line and bar chart for N1 and N2, respectively. **g-j** Specific activity (malate dehydrogenase (MDH), pyruvate carboxylase (PYC), glutamine synthase (GS), and glutamate synthase (GOGAT) of FMME218-37 and the mutant strain FMME-S-38

insight into the nutrient content required to enhance the production of targeted metabolites.

In this study, the PVM and compactness of the colony were first used to characterize the L-malate production capacity of mutants on the plate. As a result, a mutant FMME-S-38 exhibiting denser conidia, thicker conidia stalks, and smoother pellets than those of the parent strain was isolated and could produce 79.8 g/L L-malate. These morphological characteristics are very similar to those reported for a high-producing *A. niger* strain in citric acid fermentation (Sun et al. 2018). As the pellet and colony morphologies are important physiological parameters of filamentous fungi, manipulating these represents an efficient approach to enhance the production of targeted metabolites using fungal strains. Optimizing the pellet morphology of filamentous fungi in submerged culture could ensure higher oxygen mass transfer and nutrient absorption from the fermentation broth, thus enhancing production of the targeted metabolite by *Rhizopus oryzae* (Longacre et al. 1997), *A. niger* (Papagianni 2007), *Aspergillus terreus* (Porcel et al. 2005), and *A. oryzae* (Chen et al. 2019; Ding et al. 2018). Moreover, the parameters of colony morphology include the spore color, colony color, colony diameter, colony furrows, and colonial growth rate, which play a vital role in the synthesis capability of filamentous fungi. For example, in a previous study, the spore color, colonial growth rate, and formation of pigments on the plate were used to characterize the β-1,4-endoxylanase activity in *A. niger*, and this colony selection method was combined with γ-ray-induced mutagenesis to isolate the mutants with high enzyme activities (Ottenheim et al. 2015). In addition, the diameter and color of the colony

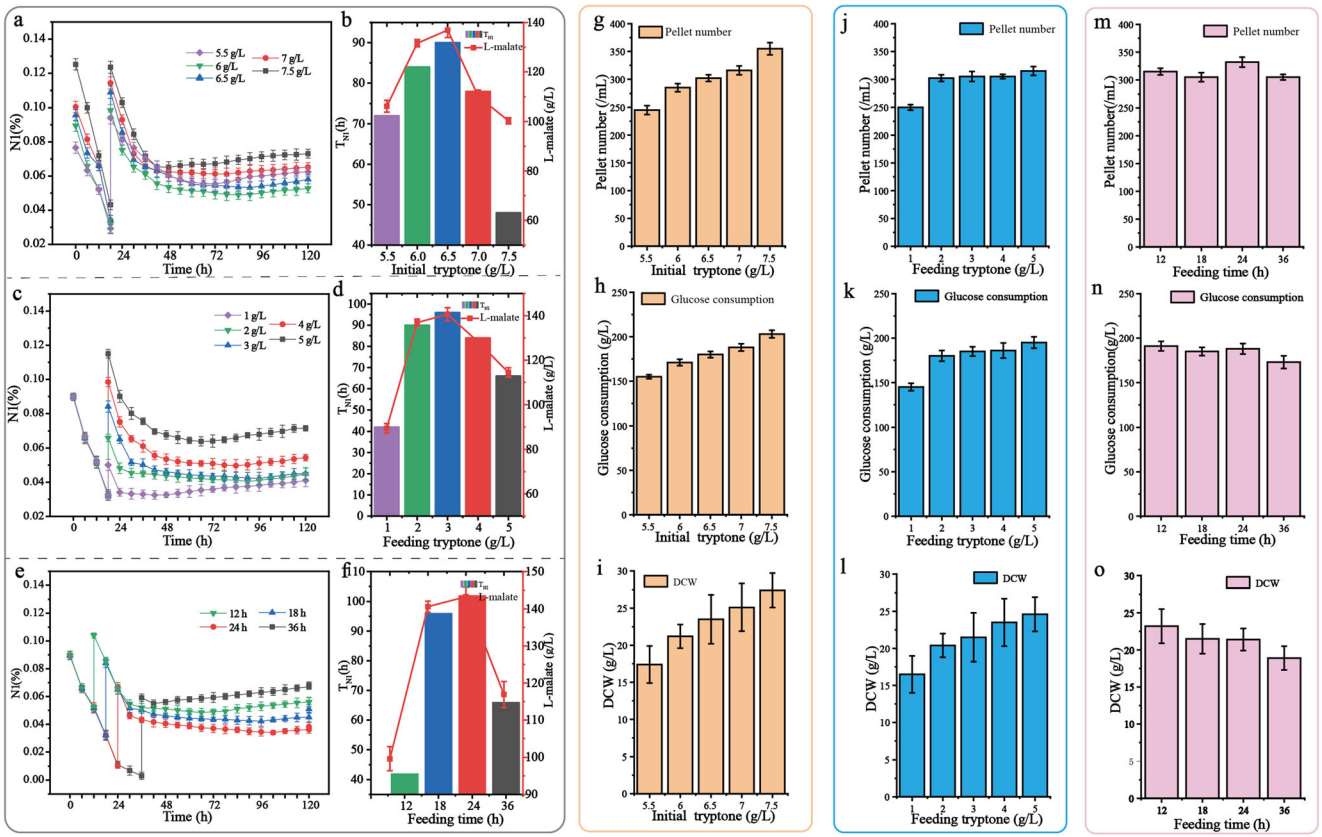

Fig. 4 Nitrogen supply optimization strategy based on tuning the initial tryptone concentration (as the nitrogen source), feeding tryptone concentration, and of tryptone feeding time. **a**–**f** Curve of extracellular nitrogen content (N1) to optimize the nitrogen supply strategy for 120 h, and the relationship between the T_{N1} value and L-malate production. **g-i** Influence of initial tryptone concentration on changes in glucose consumption, pellet size, and dry cell weight (DCW). **j-l** Influence of feeding concentration of tryptone on the change of glucose consumption, pellet size, and DCW. **m-o** Influence of the feeding time of tryptone on the change of glucose consumption, pellet size, and DCW affected by the feeding time of tryptone

were used as morphological characteristics to isolate an *Actinoplanes teicomyceticus* strain with a higher teicoplanin production ability (Lee et al. 2003). The number of colony furrows was also used to characterize the histidine synthesis ability of *Salmonella typhimurium* (Adrio & Demain 2006) and the oxygen tolerance ability of *Aspergillus fumigatus* (Kowalski et al. 2019). These examples present a guide on how to isolate the high-producing fungal strains; however, a clear and complete set of morphological characteristics for high-producing strains has not yet been elucidated.

According to the curves of N1 and N2, the fermentation process of L-malate was divided into the growth stage, rapid acid-producing stage, and self-dissolving stage. The T_{N1} and T_{N2} values could be used as an indicator to increase the duration of the rapid acid-producing stage; as a result, the L-malate titer was further enhanced. In *Spirulina platensis*, the change in nitrogen utilization capacity also acts as an indicator to switch the different fermentation stages (Li et al. 2018a). The method of dividing the fermentation process differed from previous studies, in which the fermentation process was divided into different stages according to the kinetic parameters (e.g., specific growth rate, specific substrate consumption rate, and specific product formation rate) and target metabolite synthesis capacity. This was done to control the environmental conditions (pH-, temperature-, DO-, etc.) at a suitable level for cell growth or product synthesis (Li et al. 2002; Pan et al. 2017; Yu et al. 2016; Zhao et al. 2015). For example, based on the changes in the specific growth rate and the poly L-lysine synthesis capacity in *Streptomyces albulus*, a pH stage-controlled strategy (initial pH 5.0, decreased to 3.85 over 12 h after a slight increase) was developed to increase the poly L-lysine titer by 32.3% (Pan et al. 2017). Similarly, DO and temperature control strategies were developed to efficiently increase the production of pyruvate (from 0.91 to 1.24 g/L/h), L-tryptophan titer (by 19.3%), and pullulan yield (by 18.18%) (Adrio & Demain 2006; Cao et al. 2012; Li et al. 2002). The strategy presented here may provide a potential method to further increase the production of metabolites with different strains.

In this study, an optimal nitrogen supply strategy was developed to increase the T_{N1} value from 78 to 114 h in a 30-L fermentor, based on the relationship between T_{N1}, T_{N2}, and L-

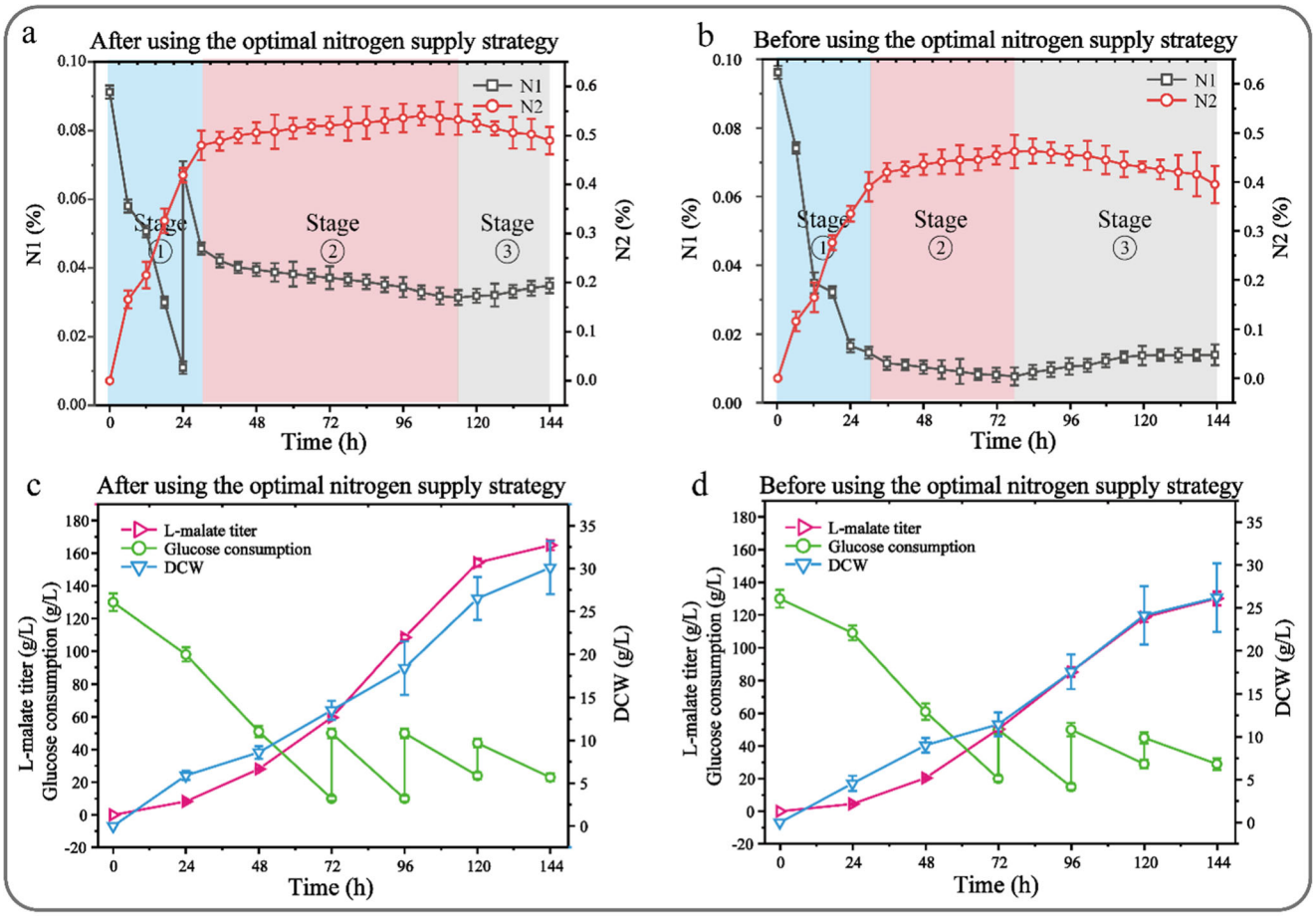

Fig. 5 Scale-up in the 30-L fermentor. a The change of N1 and N2 in the process of 30-L fermentation after using the optimal nitrogen supply strategy. **b** The change of N1 and N2 in the process of 30-L fermentation before using the optimal nitrogen supply strategy. **c** Fermentation parameters of *A.oryzae* FMME-S-38 in the 30-L fermentor after using the optimal nitrogen supply strategy. **d** Fermentation parameters of *A.oryzae* FMME-S-38 in the 30-L fermentor before using the optimal nitrogen supply strategy. Data points reflect the average of three independent fermentation processes, with error bars representing the standard deviation. **e** The morphology of pellets after using the optimal nitrogen supply strategy in the 7.5-L fermentor and 30-L fermentor

malate production. The use of this strategy led to an increase in the L-malate titer from 130.5 to 164.9 g/L. Nitrogen is an important nutrient for industrial strains, and early studies mainly focused on selecting the nitrogen source and optimizing the nitrogen content. For example, $(NH_4)_2HPO_4$ was reported to be the most suitable nitrogen source for enhancing curdlan production by *Rhizobium radiobacter*, and the optimum concentration (5.5 g/L) and addition time (9 h) were further established to ultimately increase the curdlan titer by 210% (Wang et al. 2016). Subsequently, several researchers focused on developing appropriate nitrogen starvation strategies (Chu et al. 2020; Gao et al. 2013; Knuf et al. 2013; Li

et al. 2018a) or to control the optimum C/N ratio (Ling et al. 2015; Wang et al. 2016) for enhancing the microbial metabolite production. One good example is that fatty acids could be accumulated without citric acid excretion within a C/N ratio change rate of 47.6–58.8 Cmol $Nmol^{-1}$ (Sagnak et al. 2018). This study demonstrated that tuning the C/N ratio not only enhances the targeted metabolite production (Carsanba et al. 2019; Ding et al. 2018; Liu et al. 2020) but also eliminates by-product formation. However, to our best knowledge, the impact of N1 and N2 levels on the physiological function and production efficiency of industrial strains remains unclear. In this study, a clear correlation was observed between the N1 and N2 contents and L-malate production by *A. oryzae*, and nitrogen supply strategies were developed to increase the L-malate titer in both 7.5- and 30-L fermentors. Our findings demonstrate the potential of this strategy for industrial scale-up to improve the production of L-malate and similar metabolites.

Author contribution Ji L and Luo Q conceived and designed research. Ji L and Wang J conducted experiments. Ji L analyzed the data and wrote the manuscript. Wang J, Ding Q, and Tang W contributed with scientific discussions and commented on the manuscript. Chen X and Liu L supervised the work and revised the manuscript. All authors read and approved the manuscript.

Funding This work was financially supported by the Key Program of the National Natural Science Foundation of China (22038005), the National Key R & D Program of China (2018YFA0901400, 2020YFA0908500), the General Program of National Natural Science Foundation of China (21978113), and the national first-class discipline program of Light Industry Technology and Engineering (LITE2018-08).

Data availability The data that support the figures within this paper and other findings of this study are available from the corresponding author upon reasonable request.

Declarations

Ethical approval This article does not contain any studies on human participants or animals performed by any of the authors.

Conflict of interest The authors declare that they have no competing interests.

References

Adrio JL, Demain AL (2006) Genetic improvement of processes yielding microbial products. FEMS Microbiol Rev 30(2):187–214. https://doi.org/10.1111/j.1574-6976.2005.00009.x

Battat E, Peleg Y, Bercovitz A, Rokem JS, Goldberg I (1991) Optimization of L-malic acid production by *Aspergillus flavus* in a stirred fermenter. Biotechnol Bioeng 37(11):1108–1116. https://doi.org/10.1002/bit.260371117

Brown SH, Bashkirova L, Berka R, Chandler T, Doty T, McCall K, McCulloch M, McFarland S, Thompson S, Yaver D, Berry A (2013) Metabolic engineering of *Aspergillus oryzae* NRRL 3488 for increased production of L-malic acid. Appl Microbiol Biotechnol 97(20):8903–8912. https://doi.org/10.1007/s00253-013-5132-2

Cao WF, Luo JQ, Zhao J, Qiao CS, Ding LH, Qi BK, Su Y, Wan YH (2012) Intensification of beta-poly(L: -malic acid) production by *Aureobasidium pullulans* ipe-1 in the late exponential growth phase. J Ind Microbiol Biotechnol 39(7):1073-80. https://doi.org/10.1007/s10295-012-1111-3

Carsanba E, Papanikolaou S, Fickers P, Erten H (2019) Screening various *Yarrowia lipolytica* strains for citric acid production. Yeast 36(5):319-327. https://doi.org/10.1002/yea.3389

Chen XL, Wang YC, Dong XX, Hu GP, Liu LM (2017) Engineering rTCA pathway and C4-dicarboxylate transporter for L-malic acid production. Appl Microbiol Biotechnol 101(10):4041-4052. https://doi.org/10.1007/s00253-017-8141-8

Chen XL, Xu GQ, Xu N, Zou W, Zhu P, Liu LM, Chen J (2013) Metabolic engineering of *Torulopsis glabrata* for malate production. Metab Eng 19:10-16. https://doi.org/10.1016/j.ymben.2013.05.002

Chen XL, Zhou J, Ding Q, Luo QL, Liu LM (2019) Morphology engineering of *Aspergillus oryzae* for L-malate production. Biotechnol Bioeng 116(10):2662-2673. https://doi.org/10.1002/bit.27089

Chi Z, Wang ZP, Wang GY, Khan I, Chi ZM (2016) Microbial biosynthesis and secretion of L-malic acid and its applications. Crit Rev Biotechnol 36(1):99–107. https://doi.org/10.3109/07388551.2014.924474

Christensen T, Hynes MJ, Davis MA (1998) Role of the regulatory gene *areA* of *Aspergillus oryza*e in nitrogen metabolism. Appl Environ Microbiol 64(9):3232-3237.

Chu FF, Cheng J, Li K, Wang YG, Li X, Yang WJ (2020) Enhanced lipid accumulation through a regulated metabolic pathway of phosphorus luxury uptake in the microalga *Chlorella Vulgaris* under nitrogen starvation and phosphorus depletion. ACS Sustain Chem Eng 8(22):8137-8147. https://doi.org/10.1021/acssuschemeng.9b07447

Ding H, Inoue S, Ljubimov AV, Patil R, Portilla Arias J, Hu J, Konda B, Wawrowsky KA, Fujita M, Karabalin N, Sasaki T, Black KL, Holler E, Ljubimova JY (2010) Inhibition of brain tumor growth by intravenous poly (beta-L-malic acid) nanobioconjugate with pH-dependent drug release. Proc Natl Acad Sci U S A 107(42):18143-18148. https://doi.org/10.1073/pnas.1003919107

Ding Q, Luo QL, Zhou J, Chen XL, Liu LM (2018) Enhancing L-malate production of *Aspergillus oryzae* FMME218-37 by improving inorganic nitrogen utilization. Appl Microbiol Biotechnol 102(20):8739-8751. https://doi.org/10.1007/s00253-018-9272-2

Dong XX, Chen XL, Qian YY, Wang YC, Wang L, Qiao WH, Liu LM (2017) Metabolic engineering of *Escherichia coli* W3110 to produce L-malate. Biotechnol Bioeng 114(3):656-664. https://doi.org/10.1002/bit.26190

Downes DJ, Dayis MA, Kreutzberger SD, Taig BL, Todd RB (2013) Regulation of the NADP-glutamate dehydrogenase gene *gdhA* in *Aspergillus nidulans* by the Zn(II)2Cys6 transcription factor LeuB. Microbiology-Sgm 159(12):2467-2480. https://doi.org/10.1099/mic.0.071514-0

Gao C, Wang SH, Hu GP, Guo L, Chen XL, Xu P, Liu LM (2018) Engineering *Escherichia coli* for malate production by integrating modular pathway characterization with CRISPRi-guided multiplexed metabolic tuning. Biotechnol Bioeng 115(3):661-672. https://doi.org/10.1002/bit.26486

Gao YY, Yang MC, Wang CH (2013) Nutrient deprivation enhances lipid content in marine microalgae. Bioresour Technol 147:484-491. https://doi.org/10.1016/j.biortech.2013.08.066

Guo L, Zhang F, Zhang C, Hu GP, Gao C, Chen XL, Liu LM (2018) Enhancement of malate production through engineering of the periplasmic rTCA pathway in *Escherichia coli*. Biotechnol Bioeng 115(6):1571-1580. https://doi.org/10.1002/bit.26580

Harper M, Lee CJ (2012) Genome-wide analysis of mutagenesis bias and context sensitivity of N-methyl-N'-nitro-N-nitrosoguanidine (NTG). Mutat Res 731(1-2):64-7. https://doi.org/10.1016/j.mrfmmm.2011.10.011

Hu GP, Zhou J, Chen XL, Qian YY, Gao C, Guo L, Xu P, Chen W, Chen J, Li Y, Liu LM (2018) Engineering synergetic CO_2-fixing pathways for malate production. Metab Eng 47:496-504. https://doi.org/10.1016/j.ymben.2018.05.007

Huang DM, Song YY, Liu YL, Qin Y (2019) A new strain of *Aspergillus tubingensis* for high-activity pectinase production. Braz J Microbiol 50(1):53-65. https://doi.org/10.1007/s42770-018-0032-3

Iyyappan J, Baskar G, Gnansounou E, Pandey A, Raaman JK, Bharathiraja B, Praveenkumar R (2019) Recent advances in microbial production of malic acid from renewable byproducts. Rev Environ Sci Bio-Technol 18(3):579-595. https://doi.org/10.1007/s11157-019-09503-2

Jantama K, Haupt MJ, Svoronos SA, Zhang X, Moore JC, Shanmugam KT, Ingram LO (2008) Combining metabolic engineering and metabolic evolution to develop nonrecombinant strains of *Escherichia coli* C that produce succinate and malate. Biotechnol Bioeng 99(5):1140-53. https://doi.org/10.1002/bit.21694

Karahalil E, Coban HB, Turhan I (2019) A current approach to the control of filamentous fungal growth in media: microparticle enhanced cultivation technique. Crit Rev Biotechnol 39(2):192–201. https://doi.org/10.1080/07388551.2018.1531821

Khan I, Nazir K, Wang ZP, Liu GL, Chi ZM (2014) Calcium malate overproduction by *Penicillium viticola* 152 using the medium containing corn steep liquor. Appl Microbiol Biotechnol 98(4):1539-1546. https://doi.org/10.1007/s00253-013-5326-7

Knuf C, Nookaew I, Brown SH, McCulloch M, Berry A, Nielsen J (2013) Investigation of malic acid production in *Aspergillus oryzae* under nitrogen starvation conditions. Appl Environ Microbiol 79(19):6050-6058. https://doi.org/10.1128/aem.01445-13

Kövilein A, Kubisch C, Cai L, Ochsenreither K (2019) Malic acid production from renewables: a review. J Chem Technol Biotechnol 95(3):513–526. https://doi.org/10.1002/jctb.6269

Kowalski CH, Kerkaert JD, Liu KW, Bond MC, Hartmann R, Nadell CD, Stajich JE, Cramer RA (2019) Fungal biofilm morphology impacts hypoxia fitness and disease progression. Nat Microbiol 4(12):2430-2441. https://doi.org/10.1038/s41564-019-0558-7

Kuck U, Hoff B (2010) New tools for the genetic manipulation of filamentous fungi. Appl Microbiol Biotechnol 86(1):51-62. https://doi.org/10.1007/s00253-009-2416-7

Kuypers MMM, Marchant HK, Kartal B (2018) The microbial nitrogen-cycling network. Nat Rev Microbiol 16(5):263-276. https://doi.org/10.1038/nrmicro.2018.9

Lee JC, Park HR, Park DJ, Son KH, Yoon KH, Kim YB, Kim CJ (2003) Production of teicoplanin by a mutant of *Actinoplanes teicomyceticus*. Biotechnol Lett 25(7):537-540. https://doi.org/10.1023/a:1022842203917

Li XJ, Liu Y, Yang Y, Zhang H, Wang HL, Wu Y, Zhang M, Sun T, Cheng JS, Wu XF, Pan LJ, Jiang ST, Wu HW (2014) High levels of malic acid production by the bioconversion of corn straw hydrolyte using an isolated *Rhizopus delemar* strain. Biotechnol Bioprocess Eng 19(3):478-492. https://doi.org/10.1007/s12257-014-0047-z

Li XT, Li W, Zhai J, Wei HX (2018a) Effect of nitrogen limitation on biochemical composition and photosynthetic performance for fed-batch mixotrophic cultivation of microalga *Spirulina platensis*. Bioresour Technol 263:555-561. https://doi.org/10.1016/j.biortech.2018.05.046

Li Y, Hugenholtz J, Chen J, Lun SY (2002) Enhancement of pyruvate production by *Torulopsis glabrata* using a two-stage oxygen supply control strategy. Appl Microbiol Biotechnol 60(1-2):101-6. https://doi.org/10.1007/s00253-002-1064-y

Li ZJ, Hong PH, Da YY, Li LK, Stephanopoulos G (2018b) Metabolic engineering of *Escherichia coli* for the production of L-malate from xylose. Metab Eng 48:25-32. https://doi.org/10.1016/j.ymben.2018.05.010

Lim J, Choi YH, Hurh BS, Lee I (2019) Strain improvement of *Aspergillus sojae* for increased L-leucine aminopeptidase and protease production. Food Sci Biotechnol 28(1):121-128. https://doi.org/10.1007/s10068-018-0427-9

Ling XP, Guo J, Liu XT, Zhang X, Wang N, Lu YH, Ng IS (2015) Impact of carbon and nitrogen feeding strategy on high production of biomass and docosahexaenoic acid (DHA) by *Schizochytrium* sp. LU310. Bioresour Technol 184:139-147. https://doi.org/10.1016/j.biortech.2014.09.130

Liu JJ, Xie ZP, Shin H-D, Li JH, Du GC, Chen J, Liu L (2017) Rewiring the reductive tricarboxylic acid pathway and L-malate transport pathway of *Aspergillus oryzae* for overproduction of L-malate. J Biotechnol 253:1-9. https://doi.org/10.1016/j.jbiotec.2017.05.011

Liu XY, Yu XJ, Wang ZP, Xia J, Yan YB, Hu L, Wang XY, Xu JX, He AY, Zhao PS (2020) Enhanced erythritol production by a Snf1-deficient *Yarrowia lipolytica* strain under nitrogen-enriched fermentation condition. Food Bioprod Process 119:306-316. https://doi.org/10.1016/j.fbp.2019.11.012

Longacre A, Reimers JM, Gannon JE, Wright BE (1997) Flux analysis of glucose metabolism in *Rhizopus oryzae* for the purpose of increasing lactate yields. Fungal Genet Biol 21(1):30–39. https://doi.org/10.1006/fgbi.1996.0952

Ottenheim C, Werner KA, Zimmermann W, Wu JC (2015) Improved endoxylanase production and colony morphology of *Aspergillus niger* DSM 26641 by γ-ray induced mutagenesis. Biochem Eng J 94:9-14. https://doi.org/10.1016/j.bej.2014.10.020

Pan L, Chen XS, Liu MM, Liu YJ, Mao ZG (2017) Efficient production of epsilon-poly-L-lysine from glucose by two-stage fermentation using pH shock strategy. Process Biochem 63:8-15. https://doi.org/10.1016/j.procbio.2017.08.008

Papagianni M (2007) Advances in citric acid fermentation by *Aspergillus niger*: biochemical aspects, membrane transport and modeling. Biotechnol Adv 25(3):244-63. https://doi.org/10.1016/j.biotechadv.2007.01.002

Porcel EMR, Lopez JLC, Perez JAS, Sevilla JMF, Chisti Y (2005) Effects of pellet morphology on broth rheology in fermentations of *Aspergillus terreus*. Biochem Eng J 26(2-3):139-144. https://doi.org/10.1016/j.bej.2005.04.011

Rokem JS, Lantz AE, Nielsen J (2007) Systems biology of antibiotic production by microorganisms. Nat Prod Rep 24(6):1262-1287. https://doi.org/10.1039/b617765b

Sagnak R, Cochot S, Molina-Jouve C, Nicaud J-M, Guillouet SE (2018) Modulation of the glycerol phosphate availability led to concomitant reduction in the citric acid excretion and increase in lipid content and yield in *Yarrowia lipolytica*. J Biotechnol 265:40-45. https://doi.org/10.1016/j.jbiotec.2017.11.001

Sun XW, Wu HF, Zhao GH, Li ZM, Wu XH, Liu H, Zheng ZM (2018) Morphological regulation of *Aspergillus niger* to improve citric acid production by *chsC* gene silencing. Bioprocess Biosyst Eng 41(7):1029-1038. https://doi.org/10.1007/s00449-018-1932-1

Swift RJ, Craig SH, Wiebe MG, Robson GD, Trinci APJ (2000) Evolution of *Aspergillus niger* and *A. nidulans* in glucose-limited chemostat cultures, as indicated by oscillations in the frequency of cycloheximide resistant and morphological mutants. Mycol Res 104(3):333-337. https://doi.org/10.1017/S0953756299001136

Wakai S, Yoshie T, Asai Nakashima N, Yamada R, Ogino C, Tsutsumi H, Hata Y, Kondo A (2014) L-lactic acid production from starch by simultaneous saccharification and fermentation in a genetically engineered *Aspergillus oryzae* pure culture. Bioresour Technol 173:376-383. https://doi.org/10.1016/j.biortech.2014.09.094

Wang XYZ, Dong JJ, Xu GC, Han RZ, Ni Y (2016) Enhanced curdlan production with nitrogen feeding during polysaccharide synthesis by *Rhizobium radiobacter*. Carbohydr Polym 150:385-391. https://doi.org/10.1016/j.carbpol.2016.05.036

Xu YX, Zhou YT, Cao W, Liu H (2020) Improved production of malic acid in *Aspergillus niger* by abolishing citric acid accumulation and enhancing glycolytic flux. ACS Synth Biol 9(6):1418-1425. https://doi.org/10.1021/acssynbio.0c00096

Yu XH, Zhu XM, Lin XW, Li FW, Gu ZX (2016) Effects of two-stage controlled pH and temperature vs. one-step process for hemicellulase biosynthesis and feruloyl oligosaccharide fermentation using *Aureobasidium pullulans*. Bioresources 11(2):5113-5123.

Zambanini T, Kleineberg W, Sarikaya E, Buescher JM, Meurer G, Wierckx N, Blank LM (2016) Enhanced malic acid production from glycerol with high-cell density *Ustilago trichophora* TZ1 cultivations. Biotechnol Biofuels 9(135):1-10. https://doi.org/10.1186/s13068-016-0553-7

Zelle RM, de Hulster E, van Winden WA, de Waard P, Dijkema C, Winkler AA, Geertman JM, van Dijken JP, Pronk JT, van Maris AJ (2008) Malic acid production by *Saccharomyces cerevisiae*: engineering of pyruvate carboxylation, oxaloacetate reduction, and malate export. Appl Environ Microbiol 74(9):2766-77. https://doi.org/10.1128/AEM.02591-07

Zhang X, Wang X, Shanmugam KT, Ingram LO (2011) L-malate production by metabolically engineered *Escherichia coli*. Appl Environ Microbiol 77(2):427–34. https://doi.org/10.1128/AEM.01971-10

Zhang ZY, Jin B, Kelly JM (2007) Production of lactic acid and byproducts from waste potato starch by *Rhizopus arrhizus*: role of nitrogen sources. World J Microbiol Biotechnol 23(2):229-236. https://doi.org/10.1007/s11274-006-9218-1

Zhao CG, Cheng LK, Xu QY, Wang J, Shen ZQ, Chen N (2015) Improvement of the production of L-tryptophan in *Escherichia coli* by application of a dissolved oxygen stage control strategy. Ann Microbiol 66(2):843–854. https://doi.org/10.1007/s13213-015-1172-4